JACS
JOURNAL OF THE AMERICAN CHEMICAL SOCIETY
Communication
pubs.acs.org/JACS

C and N Hybrid Coordination Derived Co−C−N Complex as a Highly Efficient Electrocatalyst for Hydrogen Evolution Reaction

Zhong-Li Wang,[†,§] Xian-Feng Hao,[‡,§] Zheng Jiang,[∥] Xue-Ping Sun,[∥] Dan Xu,[†] Jun Wang,[†] Hai-Xia Zhong,[†] Fan-Lu Meng,[†] and Xin-Bo Zhang*[,†]

[†]State Key Laboratory of Rare Earth Resource Utilization, Changchun Institute of Applied Chemistry, Chinese Academy of Sciences, Changchun, 130022, China

[‡]Key Laboratory of Applied Chemistry, Yanshan University, Qinhuangdao, 066004, China

[∥]Shanghai Synchrotron Radiation Facility, Shanghai Institute of Applied Physics, Chinese Academy of Sciences, Shanghai, 201204, China

Supporting Information

ABSTRACT: Development of an efficient hydrogen evolution reaction (HER) catalyst composed of earth-abundant elements is scientifically and technologically important for the water splitting associated with the conversion and storage of renewable energy. Herein we report a new class of Co−C−N complex bonded carbon (only 0.22 at% Co) for HER with a self-supported and three-dimensional porous structure that shows an unexpected catalytic activity with low overpotential (212 mV at 100 mA cm^{-2}) and long-term stability, better than that of most traditional-metal catalysts. Experimental observations in combination with density functional theory calculations reveal that C and N hybrid coordination optimizes the charge distribution and enhances the electron transfer, which synergistically promotes the proton adsorption and reduction kinetics.

Driven by growing concerns about global warming and depletion of petroleum resources, developing clean and sustainable alternative energy sources represents one of the major scientific challenges of the 21 century. Hydrogen, as an abundant and renewable clean fuel, is an ideal candidate for replacing fossil fuels in the future.[1] Electrocatalytic reduction of water to molecular hydrogen via the hydrogen evolution reaction (HER) provides a promising solution for hydrogen production with high purity in large quantities, but an efficient electrocatalyst for HER is required to afford a high energetic efficiency.[2] Although noble metals such as Pt-based catalysts are the most active materials for the HER, their high costs greatly restrict the industrial production of hydrogen.[3] Therefore, exploring low-cost alternatives to noble catalysts is a key technological task in the development of the hydrogen economy. In recent years, a wide variety of transition metals (Mo, W, Co, Ni, and Fe) and derivative components (sulfides, phosphides, nitrides, borides, carbides) have been selected as effective candidates.[4−7] However, for sustainable hydrogen production, it is still urgent to decrease the usage of metal and explore new catalytic systems with little or no metal.

Carbon-based materials feature unique advantages for designated catalysis due to their tunable molecular structures, abundance, and strong tolerance to acidic/alkaline environments.[8] Recent advances in low-dimensional carbon materials have shown their promising future in energy-related electrocatalytic reactions, especially for oxygen reduction reaction (ORR).[9] After heteroatom (such as N, B, P, and S) doping, the enhanced catalysis activity of carbon materials has been widely illustrated for ORR in aqueous electrolyte.[10] In particular, the codoping of trace transition metals and N atoms to form metal−nitrogen complexes (typically Fe−N_x/C) in carbon materials has largely boosted its ORR activity. Although carbon-based materials have exhibited great success in ORR catalysis, they appear relatively primitive in HER catalysis. Recently, nitrogen-rich carbon nanotubes, nitrogen/phosphine and nitrogen/sulfur codoped graphene, and carbon nitride-loaded graphene have shown improved catalytic activity for HER.[11,12] However, the overall catalytic activity is still much lower in comparison with other Pt-free catalysts. Moreover, these electrocatalysts are generally prepared in the form of one-dimensional (1D) or 2D particles, and they are randomly aggregated when preparing electrodes. The absence of pores on such electrodes leads to limited gas transport within them. Therefore, the development of highly active sites with an optimized structural design is crucial to improve the catalytic performance of carbon-based catalysts for HER.

Here, we successfully develop a novel protocol to synthesize self-supported and 3D porous Co−C−N complex bonded carbon fiber foam by the *in situ* carbonization of a cobalt ion absorbed polyaniline (PANI) precursor on a current collector. C and N hybrid coordination derived Co−C−N complex is firstly identified as a highly active molecule catalytic center for HER. Moreover, while maintaining performance similar to that of transition-metal compounds, the amount of metal in Co−C−N is reduced by 2 orders of magnitude.

Our strategy for the synthesis of Co-C-N materials contains four simple steps: electrodeposition, ions adsorption, carbonization, and acid wash (Figure 1a and S1−S3). Figure 1b shows a low-magnification scanning electron microscopy (SEM) image, indicating that the PANI-derived carbon nanofibers with an average diameter of 500 nm are interconnected with each other,

Received: August 26, 2015
Published: November 11, 2015

ACS Publications © 2015 American Chemical Society

DOI: 10.1021/jacs.5b09021
J. Am. Chem. Soc. 2015, 137, 15070−15073

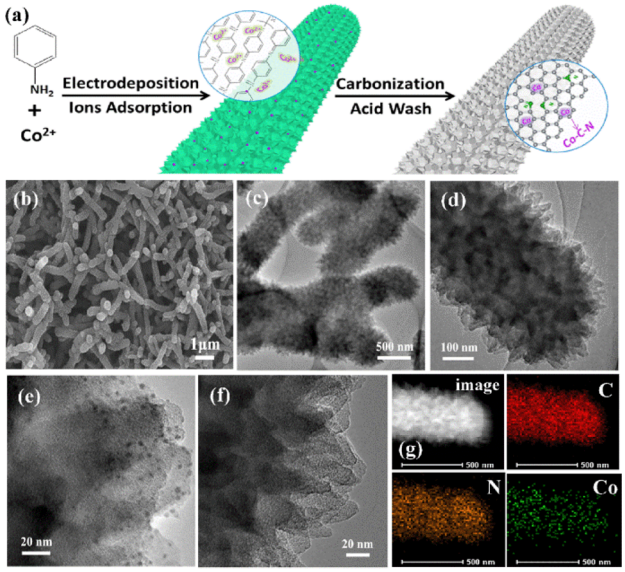

Figure 1. (a) Schematic illustration of the synthetic process; (b–d) SEM and TEM images of Co–C–N catalyst; (e, f) Comparison of before and after acid wash; and (g) STEM image and EDX elemental mapping of C, N, and Co for the Co–C–N nanofiber.

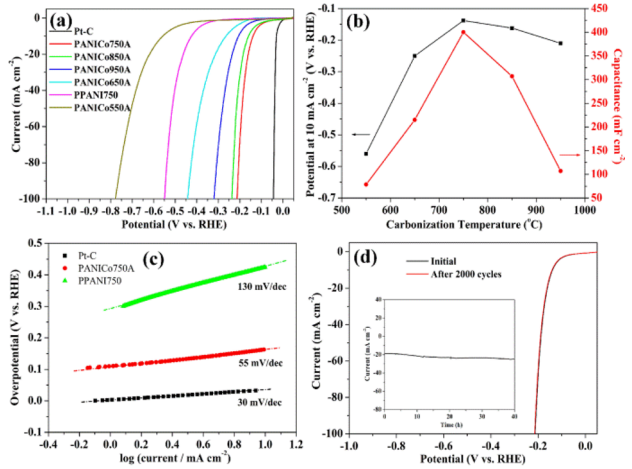

Figure 2. (a) Polarization curves of PPANI750, PANICo550-950A, and Pt/C in 0.5 M H_2SO_4. (b) Potentials at 10 mA cm^{-2} and the capacitance of the double layer as a function of the carbonization temperature. (c) Tafel plots of PANICo750A, PPANI750, and Pt/C. (d) Cycle stability measurement. Inset in (d) is the time-dependent current density curve under a constant potential of −0.17 V for 40 h.

forming a 3D macroporous structure. From the transmission electron microscopy (TEM) images of Figure 1c,d, it is clearly observed that the edge of the nanofibers is serrated, greatly enlarging the active surface area. The serrated morphology indirectly reflects the staggered stacking of the PANI nanosheets in the formation process of the PANI fibers. Figure 1e,f is the comparison of sample PANICo750 before and after acid treatment. Nanoparticles are formed on the surface of the carbon sheet, while after the acid wash, the obvious particles disappear, indicating that they are dissolved in acid. The HRTEM images further demonstrate that no cobalt compound nanoparticles or nanoclusters remain (Figure S4). However, the energy-dispersive X-ray (EDX) spectrum analysis (Figure 1g) verifies that Co and N elements are uniformly distributed in the whole fiber after the acid wash, which implies that the Co atoms are bonded with the N-doped carbon and they are stable in an acid environment. The nitrogen adsorption/desorption isotherm shows the microporous feature of carbon fibers for PANICo750A (Figure S4d). Samples prepared at other temperatures exhibit similar morphology and structure, but the diameters of the fibers become fine and the defective structures of carbon increase with the temperature (Figures S5–9). The change in the components with temperature is clearly reflected by the X-ray diffraction (XRD) spectra (Figure S10a). Interestingly, at 550 and 650 °C, there are not diffraction peaks of cobalt compounds, while at 750 °C, peaks of CoC_x are clearly observed before acid treatment. When continuously increasing temperature to 850 and 950 °C, the peaks shift from $Co_{5.47}N$ to metal Co. The different temperatures lead to different cobalt compounds, indicating that the temperature affects the interactions between Co ions and carbon support. The production of CoC_x and $Co_{5.47}N$ demonstrates that Co–C and Co–N bonds can be formed by controlling the reaction temperature. Even after an acid wash, the spectra of X-ray photoelectron spectroscopy (XPS) confirm the existence of the above bonds (Figure S10c).

Figure 2a shows the polarization curves of samples prepared at different temperatures in 0.5 M H_2SO_4 electrolyte. Commercial Pt/C and pure PANI without Co (PPANI750) are also examined for comparison. Interestingly, a slightly active N-doped carbon (PPANI750) becomes highly active with Co incorporation (PANICo750A), demonstrating the crucial role of the Co species. Moreover, the Co incorporation also makes the catalyst superhydrophilic (Figure S11). It should be noted that the content of Co is only 0.22 at% (Table S1). In contrast, the introduction of Ni or Fe plays little role for HER (Figure S12). Among the series of samples treated at different temperatures, PANICo750A exhibits the best activity. The overpotentials required to drive the cathodic current densities of 10, 20, and 100 mA cm^{-2} are 138, 160, and 212 mV, respectively. These overpotentials are among the most active for electrocatalysts based on non-noble materials (Table S2). PANICo850A exhibits a small decrease but is still much better than the other three samples. Combined with the results of XRD and XPS, it could be speculated that the great improvement in the activity in PANICo750A and PANICo850A originates from the formation of Co–C and Co–N bonds. Figure 2b shows that the potentials at 10 mA cm^{-2} first decrease and then increase with the increasing temperature from 550 to 950 °C, and the change in capacitance exhibits a similar trend (Figures S13–14). As is well-known, the capacitances of samples reflect their electrochemical surface areas. Both parabolic changes indicate that controlling the carbonization temperature can realize the maximum HER activity, at which reactions between Co ions and PANI produce large amounts of highly active sites, accompanied by the enlargement of the active surface area. Furthermore, for the polymer derived carbons, the mass of products is also greatly affected by the temperature, as shown in Figure S15a. Too high a temperature will lead to serious loss of carbon and will destroy the active components. Typically, the mass density of PANICo950A is only half that of PANICo750A, the area activity is converted into mass activity, and PANICo950A is still inferior to PANICo750A (Figure S15b). Therefore, it is crucial to select a rational carbonization temperature to balance the crystallinity of the carbon and the maximization of the active area for the polymer precursors.

The structure also plays significant role in the formation of active sites and an interesting comparable experiment is carried out. When the PANICo fiber precursor is stripped from the

DOI: 10.1021/jacs.5b09021
J. Am. Chem. Soc. 2015, 137, 15070–15073

current collector and the 3D porous structure is destroyed, the carbonized product is completely different, as shown in Figure S16. Strong diffraction peaks of CoO and Co are observed, and large particles emerge in TEM images. Moreover, after acid washing, there are almost no Co atoms remaining in the EDX mapping (Figure S17), indicating that Co atoms are not bonded with the carbon support. This experiment indicates that the disordered structure leads to the aggregation of cobalt nanoparticles to form large nanoparticles, as illustrated in Figure S18, which decreases the interaction between cobalt and carbon. The absence of Co−C/N species leads to inferior HER activity compared to PANICo750A (Figure S16a). Therefore, the *in situ* constructed 3D porous structure prevents the cobalt nanoparticles from aggregation and enhances the reaction between cobalt and support to facilitate the formation of Co−C and Co−N bonds. In summary, it can be concluded that the Co−C−N active site is the result of the synergistic interactions of the metal, temperature, and structure effects.

Figure 2c shows that PANICo750A exhibits a small Tafel slope of 55 mV dec^{-1}, which is comparable to or even smaller than those of many metal compound-based HER catalysts (Table S2). This Tafel slope suggests that the HER occurs through a Volmer−Heyrovsky mechanism, in which the fast discharge of a proton is followed by a rate-limiting electrochemical recombination with an additional proton.[11c] In contrast, the Tafel slope of PPANI750 is as high as 130 mV dec^{-1}. The durability of the Co−C−N catalyst is examined by continuous CV scanning. No change in the polarization curve of PANICo750A after 2000 cycles is observed (Figure 2d), suggesting the stable HER electrocatalysis of the material in acid. In addition, the catalyst can maintain a stable HER current density at ∼20 mA cm^{-2} for 40 h at a constant voltage of −0.17 V versus RHE in 0.5 M H_2SO_4 (inset of Figure 2d), and the structures of the catalyst are well preserved after the durability measurements (Figure S19). The Co−C−N catalyst also exhibits excellent catalytic activity and durability under neutral and basic conditions, with 100% Faradaic efficiency (Figures S20−22 and Tables S3−4).

The structure of the active sites is investigated by X-ray absorption near-edge structure (XANES) and extended X-ray absorption fine structure (EXAFS) spectroscopies. From the Co K-edge XANES spectra of samples treated at different temperatures and the references (Figure S23), it can be observed that PANICo750P and PANICo850P exhibit typical mixture valences (0∼+2), while for PANICo950P, the characteristic peak almost becomes that of Co^0 metal, which is consistent with the results of XRD. After acid treatment, the Co K-pre-edges of PANICo750A and PANICo850A are close to the reference of CoO (Co^{2+}, inset of Figure 3a), suggesting that the stable valence states are around +2 in the Co complex catalyst. However, the whole curves are obviously different from those of CoO and metal Co, indicating the possible existence of the Co−C/N species. Interestingly, PANICo750A and PANICo850A (Figure 3a, green and blue curves) exhibit a higher half-edge energy than samples prepared at low temperatures, which may be caused by a negative charge transfer from cobalt to carbon or nitrogen to form Co−C or Co−N bonds,[13] consistent with the results of XPS. PANICo950A still exhibits the characteristic peak of Co^0 because some metal particles are coated in graphite carbon at high temperature and they cannot be removed by acid as shown in Figure S6. The bonding environment of the Co atoms is investigated by Fourier transformed k^3-weighted EXAFS at the Co edge for PANICo750A and PANICo850A (Figure 3b). The results show that Co−C/O and Co−N/O bonding is found and their coordination numbers were estimated to be ∼3 and ∼2, respectively (Table S5). This result demonstrates that Co−C and Co−N bonds coexist to jointly form an active Co complex.

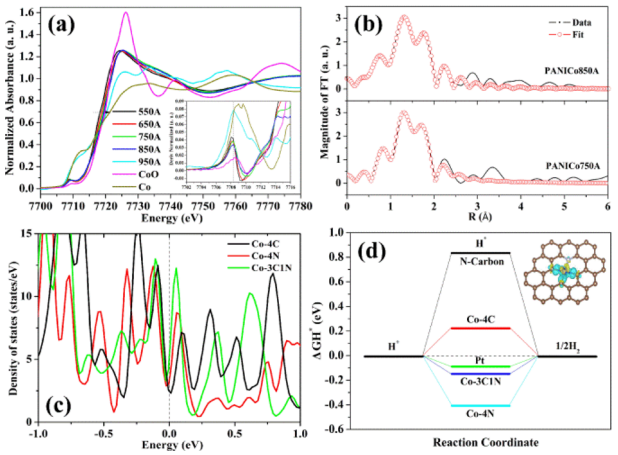

Figure 3. (a) Normalized XANES spectra near the Co K-edge of Co−C−N samples prepared at different temperatures after acid washing, and Co K-pre-edges enlarged in the inset. (b) FT-EXAFS spectra at the Co K-edge of PANICo750A and PANICo850A and their fitted curves. (c) Density of states of Co−3C1N, Co−4C, and Co−4N complexes. (d) Calculated free-energy diagram of HER at the equilibrium potential for the four catalysts, and the inset is the model structure of the Co−3C1N catalyst.

The density functional theory calculations are performed to investigate the mechanisms of the C and N hybrid coordination enhanced HER catalysis. According to the XAFS results, the total coordination number is five. It is well-known that oxygen is extremely inclined to absorb or bond on the active surface of the catalyst, which can be reflected by the first polarization curve with extra negative current (Figure S24). By assuming one coordination of bonded O_2, we construct a structure model of one cobalt ion coordinated with three C atoms and one N atom on a graphene (Figure S25). Interestingly, the optimized bond lengths of three Co−C bonds and one Co−N bond are 1.910, 1.924, 1.933, and 1.999 Å, respectively, consistent with the results of XAFS, suggesting that the model is reasonable. For comparison, the models of one cobalt ion coordinated with four C atoms or four N atoms are also calculated. From the density of states of the three models (Figure 3c), it is found that the 3C1N hybrid coordination system delivers a high density of states crossing the Fermi level, indicating enhanced electron mobility in the 3C1N complex compared to the 4N and 4C coordinated complexes. The overall HER mechanism is evaluated with a three-state diagram consisting of an initial H^+ state, an intermediate H* state, and $1/2H_2$ as the final product. A good catalyst should have a moderate free energy for H adsorption (ΔGH*) to compromise the reaction barriers of the adsorption and desorption steps. Among the graphene-based models, N-doped graphene shows a positive ΔGH* value (0.84 eV), representing a low HER activity. Co incorporation in the three models really reduces the ΔGH* values to enhance the initial H* adsorption, especially for the Co−3C1N complex with the best ΔGH* value of −0.15 eV (Figure 3d). Owing to its different electronegativity, the 4C coordination complex exhibits a relatively high charge density in the Co active site, which facilitates the desorption of H*, while for the 4N coordination complex, a low charge density is favorable to the adsorption of H*.[11b] When combining both coordinations into one complex,

DOI: 10.1021/jacs.5b09021
J. Am. Chem. Soc. 2015, 137, 15070−15073

the optimized charge distribution results in an ideal value of ΔGH* in Co−3C1N hybrid system, much better than the single or mixture system of Co−4C and Co−4N (Figure S26). Therefore, the C and N hybrid coordination synergistically enhances the activity, stability, and conductivity.

In conclusion, we have synthesized a new class of metal-heteroatom complex (Co−C−N) bonded carbon catalysts with high activity toward HER at all pH values. This work provides a new way to design advanced carbon catalysts with little metal for water splitting, fuel cells, and other electrochemical devices.

■ ASSOCIATED CONTENT

Supporting Information

The Supporting Information is available free of charge on the ACS Publications website at DOI: 10.1021/jacs.5b09021.

Details of synthesis, characterization, and theoretical calculations; Figures S1−26; and Tables S1−5 (PDF)

■ AUTHOR INFORMATION

Corresponding Author

*xbzhang@ciac.ac.cn

Author Contributions

§These authors contributed equally.

Notes

The authors declare no competing financial interest.

■ ACKNOWLEDGMENTS

This work is financially supported by 100 Talents Program of Chinese Academy of Sciences, National Program on Key Basic Research Project of China (973 Program, grant nos. 2012CB215500 and 2014CB932300), National Natural Science Foundation of China (grant nos. 21422108, 21471146, and 21203176), The Jilin Province Science and Technology Development Program (grant nos. 20140101116JC and 20150520008JH), The Jiangsu Province Basic Research Program (grant no. BK20140267). The authors thank beamline BL14W1 (Shanghai Synchrotron Radiation Facility) for the beam time.

■ REFERENCES

(1) (a) Kanan, M. W.; Nocera, D. G. *Science* **2008**, *321*, 1072. (b) Chen, Z. B.; Cummins, D.; Reinecke, B. N.; Clark, E.; Sunkara, M. K.; Jaramillo, T. F. *Nano Lett.* **2011**, *11*, 4168. (c) Cobo, S.; Heidkamp, J.; Pierre-André, J.; Fize, J.; Fourmond, V.; Guetaz, L.; Jousselme, B.; Ivanova, V.; Dau, H.; Palacin, S.; Fontecavea, M.; Artero, V. *Nat. Mater.* **2012**, *11*, 802.

(2) (a) Morales-Guio, C. G.; Hu, X. L. *Acc. Chem. Res.* **2014**, *47*, 2671. (b) Tan, C. L.; Zhang, H. *Chem. Soc. Rev.* **2015**, *44*, 2713.

(3) (a) Lv, H. F.; Xi, Z.; Chen, Z. Z.; Guo, S. J.; Yu, Y. S.; Zhu, W. L.; Li, Q.; Zhang, X.; Pan, M.; Lu, G.; Mu, S. C.; Sun, S. H. *J. Am. Chem. Soc.* **2015**, *137*, 5859. (b) Cheng, N. C.; Banis, N. B.; Liu, J.; Riese, A.; Li, X.; Li, R. Y.; Ye, S. Y.; Knights, S. N.; Sun, X. L. *Adv. Mater.* **2015**, *27*, 277.

(4) (a) Vrubel, H.; Hu, X. L. *Angew. Chem., Int. Ed.* **2012**, *51*, 12703. (b) Xie, J. F.; Zhang, J. J.; Li, S.; Grote, F.; Zhang, X. D.; Zhang, H.; Wang, R. X.; Lei, Y.; Pan, B. C.; Xie, Y. *J. Am. Chem. Soc.* **2013**, *135*, 17881. (c) Zhao, Y.; Kamiya, K.; Hashimoto, K.; Nakanishi, S. *Angew. Chem., Int. Ed.* **2013**, *52*, 13638. (d) Cao, B. F.; Veith, G. M.; Neuefeind, J. C.; Adzic, R. R.; Khalifah, P. G. *J. Am. Chem. Soc.* **2013**, *135*, 19186. (e) Wan, C.; Regmi, Y. N.; Leonard, B. M. *Angew. Chem., Int. Ed.* **2014**, *53*, 6407.

(5) (a) Popczun, E. J.; McKone, J. R.; Read, C. G.; Biacchi, A. J.; Wiltrout, A. M.; Lewis, N. S.; Schaak, R. E. *J. Am. Chem. Soc.* **2013**, *135*, 9267. (b) McEnaney, J. M.; Crompton, J. C.; Callejas, J. F.; Popczun, E. J.; Read, C. G.; Lewis, N. S.; Schaak, R. E. *Chem. Commun.* **2014**, *50*, 11026. (c) Jiang, N.; You, B.; Sheng, M.; Sun, Y. *Angew. Chem., Int. Ed.* **2015**, *54*, 6251. (d) Lukowski, M. A.; Daniel, A. S.; English, C. R.; Meng, F.; Forticaux, A.; Hamers, R. J.; Jin, S. *Energy Environ. Sci.* **2014**, *7*, 2608. (e) Kong, D. S.; Wang, H. T.; Lu, Z. Y.; Cui, Y. *J. Am. Chem. Soc.* **2014**, *136*, 4897. (f) Yang, J. U.; Voiry, D.; Ahn, S. J.; Kang, D.; Kim, A. Y.; Chhowalla, M.; Shin, H. S. *Angew. Chem., Int. Ed.* **2013**, *52*, 13751.

(6) (a) Faber, M. S.; Dziedzic, R.; Lukowski, M. A.; Kaiser, N. S.; Ding, Q.; Jin, S. *J. Am. Chem. Soc.* **2014**, *136*, 10053. (b) Yang, Y.; Fei, H. L.; Ruan, G. D.; Xiang, C. S.; Tour, J. M. *Adv. Mater.* **2014**, *26*, 8163. (c) Kong, D. S.; Cha, J. J.; Wang, H. T.; Leec, H. R.; Cui, Y. *Energy Environ. Sci.* **2013**, *6*, 3553. (d) Wang, D. Y.; Gong, M.; Chou, H. L.; Pan, C. J.; Chen, H. A.; Wu, Y. P.; Lin, M. C.; Guan, M. Y.; Yang, J.; Chen, C. W.; Wang, Y. L.; Hwang, B. J.; Chen, C. C.; Dai, H. J. *J. Am. Chem. Soc.* **2015**, *137*, 1587. (e) Gao, M. R.; Liang, J. X.; Zheng, Y. R.; Xu, Y. F.; Jiang, J.; Gao, Q.; Li, J.; Yu, S. H. *Nat. Commun.* **2015**, *6*, 5982. (f) Shalom, M.; Gimenez, S.; Schipper, F.; Herraiz-Cardona, I.; Bisquert, J.; Antonietti, M. *Angew. Chem., Int. Ed.* **2014**, *53*, 3654.

(7) (a) Zhao, Y.; Kamiya, K.; Hashimoto, K.; Nakanishi, S. *J. Am. Chem. Soc.* **2015**, *137*, 110. (b) Wu, H. B.; Xia, B. Y.; Yu, L.; Yu, X. Y.; Lou, X. W. *Nat. Commun.* **2015**, *6*, 6512. (c) Clough, A. J.; Yoo, J. W.; Mecklenburg, M. H.; Marinescu, S. C. *J. Am. Chem. Soc.* **2015**, *137*, 118. (d) Lu, Q.; Hutchings, G. S.; Yu, W. T.; Zhou, Y.; Forest, R. V.; Tao, R.; Rosen, J.; Yonemoto, B. T.; Cao, Z. Y.; Zheng, H. M.; Xiao, J. Q.; Jiao, F.; Chen, J. G. *Nat. Commun.* **2015**, *6*, 6567. (e) Kornienko, N.; Resasco, J.; Becknell, N.; Jiang, C. M.; Liu, Y. S.; Nie, K. Q.; Sun, X. H.; Guo, J. H.; Leone, S. R.; Yang, P. D. *J. Am. Chem. Soc.* **2015**, *137*, 7448. (f) Wu, R.; Zhang, J. F.; Shi, Y. M.; Liu, D. L.; Zhang, B. *J. Am. Chem. Soc.* **2015**, *137*, 6983.

(8) (a) Tang, H. J.; Yin, H. J.; Wang, J. Y.; Yang, N. L.; Wang, D.; Tang, Z. Y. *Angew. Chem., Int. Ed.* **2013**, *52*, 5585−5589. (b) Jin, H. Y.; Wang, J.; Su, D. F.; Wei, Z. Z.; Pang, Z. F.; Wang, Y. *J. Am. Chem. Soc.* **2015**, *137*, 2688. (c) Liu, Y.; Yu, G.; Li, G. D.; Sun, Y.; Asefa, T.; Chen, W.; Zou, X. *Angew. Chem., Int. Ed.* **2015**, *54*, 10752.

(9) (a) Chen, S.; Duan, J. J.; Jaroniec, M.; Qiao, S. Z. *Adv. Mater.* **2014**, *26*, 2925. (b) Deng, J.; Ren, P. J.; Deng, D. H.; Bao, X. H. *Angew. Chem., Int. Ed.* **2015**, *54*, 2100. (c) Zhuang, X. D.; Zhang, F.; Wu, D. Q.; Feng, X. L. *Adv. Mater.* **2014**, *26*, 3081.

(10) (a) Wu, G.; More, K. L.; Johnston, C. M.; Zelenay, P. *Science* **2011**, *332*, 443. (b) Lefevre, M.; Proietti, E.; Jaouen, F.; Dodelet, J. P. *Science* **2009**, *324*, 71.

(11) (a) Zou, X. X.; Huang, X. X.; Goswami, A.; Silva, R.; Sathe, B. R.; Mikmekov, E.; Asefa, T. *Angew. Chem., Int. Ed.* **2014**, *53*, 4372. (b) Zheng, Y.; Jiao, Y.; Li, L. H.; Xing, T.; Chen, Y.; Jaroniec, M.; Qiao, S. Z. *ACS Nano* **2014**, *8*, 5290. (c) Zheng, Y.; Jiao, Y.; Zhu, Y. H.; Li, L. H.; Han, Y.; Chen, Y.; Du, A. J.; Jaroniec, M.; Qiao, S. Z. *Nat. Commun.* **2014**, *5*, 3783. (d) Ito, Y.; Cong, W. T.; Fujita, T.; Tang, Z.; Chen, M. W. *Angew. Chem., Int. Ed.* **2015**, *54*, 2131.

(12) (a) Fei, H. L.; Yang, Y.; Peng, Z. W.; Ruan, G. D.; Zhong, Q. F.; Li, L.; Samuel, E. L. G.; Tour, J. M. *ACS Appl. Mater. Interfaces* **2015**, *7*, 8083. (b) Zhou, W.; Zhou, J.; Zhou, Y.; Lu, J.; Zhou, K.; Yang, L.; Tang, Z.; Ligui, L.; Chen, S. *Chem. Mater.* **2015**, *27*, 2026. (c) Liang, H. W.; Bruller, S.; Dong, R. H.; Zhang, J.; Feng, X. L.; Mullen, K. *Nat. Commun.* **2015**, *6*, 7992. (d) Morozan, A.; Goellner, V.; Nedellec, Y.; Hannauer, J.; Jaouen, F. *J. Electrochem. Soc.* **2015**, *162*, H719.

(13) (a) Chen, W. F.; Wang, C. H.; Sasaki, K.; Marinkovic, N.; Xu, W.; Muckerman, J. T.; Zhu, Y.; Adzic, R. R. *Energy Environ. Sci.* **2013**, *6*, 943. (b) Chen, W. F.; Iyer, S.; Iyer, S.; Sasaki, K.; Wang, C. H.; Zhu, Y. M.; Muckerman, J. T.; Fujita, E. *Energy Environ. Sci.* **2013**, *6*, 1818.

DOI: 10.1021/jacs.5b09021
J. Am. Chem. Soc. 2015, 137, 15070−15073